Temporal restriction of Cas9 expression improves CRISPR-mediated deletion efficacy and fidelity

Jesse A. Weber,[1,2] Jonathan F. Lang,[1,2,5] Ellie M. Carrell,[1] Mohamad-Gabriel Alameh,[4] and Beverly L. Davidson[1,3]

[1]Raymond G. Perelman Center for Cellular and Molecular Therapeutics, The Children's Hospital of Philadelphia, Philadelphia, PA, USA; [2]Cell and Molecular Biology Graduate Group, Biomedical Graduate Studies, University of Pennsylvania, Philadelphia, PA, USA; [3]Department of Pathology and Laboratory Medicine, University of Pennsylvania, Philadelphia, PA, USA; [4]Penn Institute for RNA Innovation, University of Pennsylvania, Perelman School of Medicine, Philadelphia, PA, USA

Clinical application of CRISPR-Cas9 technology for large deletions of somatic mutations is inefficient, and methods to improve utility suffer from our inability to rapidly assess mono- vs. biallelic deletions. Here we establish a model system for investigating allelic heterogeneity at the single-cell level and identify indel scarring from non-simultaneous nuclease activity at gRNA cut sites as a major barrier to CRISPR-del efficacy both *in vitro* and *in vivo*. We show that non-simultaneous nuclease activity is partially prevented via restriction of CRISPR-Cas9 expression via inducible adeno-associated viruses (AAVs) or lipid nanoparticles (LNPs). Inducible AAV-based expression of CRISPR-del machinery significantly improved mono- and biallelic deletion frequency *in vivo*, supporting the use of the X^on cassette over traditional constitutively expressing AAV approaches. These data depicting improvements to deletions and insight into allelic heterogeneity after CRISPR-del will inform therapeutic approaches for phenotypes that require either large mono- or biallelic deletions, such as autosomal recessive diseases or where mutant allele-specific gRNAs are not readily available, or in situations where the targeted sequence for excision is located multiple times in a genome.

INTRODUCTION

CRISPR-mediated deletion (CRISPR-del) of large genomic regions is a promising strategy to treat acquired and inherited diseases, for example Huntington's disease (HD), human immunodeficiency virus (HIV), and Duchenne muscular dystrophy (DMD).[1–4] CRISPR-del works by delivering Cas9 protein and guide RNAs (gRNAs) flanking the region of interest to induce double-stranded DNA breaks (DSBs) and excising the intervening region followed by non-homologous end-joining (NHEJ) DNA repair.[5–8] In contrast to introduction of small indels by single gRNA CRISPR strategies, the intent of CRISPR-del is to impair or restore gene function through the excision of larger essential or pathogenic genetic components. For example, excision of the expanded CAG repeat tract in mutant *HTT* eliminates toxic mutant huntingtin RNA and protein production, HIV provirus excision ensures removal of essential replication machinery proteins, and removal of exons containing premature stop codons in Du-

chenne's muscular dystrophy can restore appropriate translation of dystrophin-encoding mRNAs.[4,9–11] To date, CRISPR-del based approaches have not resulted in approved therapies, likely due to inefficiencies at several levels.[7,12–15]

Prior studies improved CRISPR-del frequency by pairing gRNAs with PAM-in or PAM-out orientations or modulating NHEJ-repair pathways around the time of break formation.[16,17] Data from these works suggested that the major limiting factor, at least *in vitro*, may lie in the rapid endogenous systems of DNA repair. Repair events can include indels at the two gRNA cut sites without successful deletion, inversion of the region between cut sites, or the successful full deletion.[12]

To better investigate DNA-repair outcomes resulting from CRISPR-del *in vivo* with single-cell resolution, we and others used deletion-dependent Ai14 (tdTomato) reporter mice.[18–21] However, the single-fluorophore model is blind to allelic heterogeneity (mono- vs. biallelic deletions) and revealed few successful CRISPR-del events across multiple tissues despite robust transduction.[18,19] Here, we compared the outcomes and fidelity of editing using different expression and delivery modalities for the CRISPR machinery in deletion-dependent dual-reporter Ai14/Ai6 (tdTomato/zsGreen) compound heterozygous animals, as well as cultured cells from these mice. Our findings support that restricting the CRISPR-Cas9 expression window from weeks of expression to hours (inducible expression with AAV-X^on or LNPs) significantly improves editing outcomes.

RESULTS

Single-cell resolution of allelic heterogeneity of CRISPR-del
Mouse embryonic fibroblasts (MEFs) from compound heterozygous Ai14 (tdTomato)/Ai6 (zsGreen) reporter mice were established to
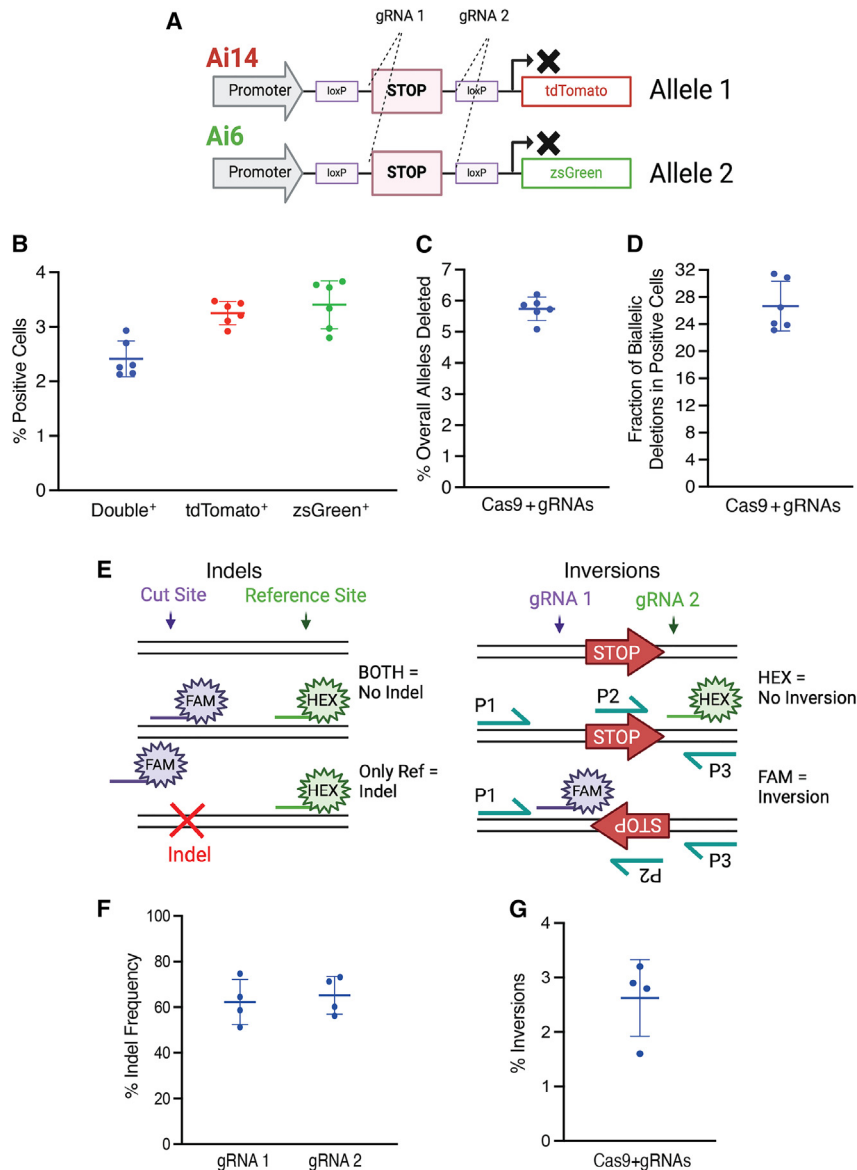
Figure 1. Single-cell resolution of allelic heterogeneity of CRISPR-del

(A) Schematic depicting the transgene cassettes of both Ai14 and Ai6 alleles, and gRNA targeting sites. (B–D) Summary of single- and double-positive cell population size, overall frequency of allelic deletions, and propensity for biallelic deletions after CRISPR-del *in vitro* using Ai14/Ai6 MEFs. (E) Schema for indel and inversion ddPCR assays. (F) Indel frequency of gRNA cut sites at non-deleted alleles assessed by ddPCR analysis. (G) Quantification of inversions via ddPCR on bulk genomic DNA from Ai14/Ai6 MEFs. Data in (B)–(D), (F), and (G) represent means ± SD.

tdTomato−) were flow sorted and PCR amplified across gRNA cut sites flanking the non-excised Ai14 STOP cassette. Sanger sequencing revealed indels at one or both cut sites (68%), inversions (20%), and indel-free sequences (12%) (Figure S1B). Additionally, indel frequencies or inversions were assessed by a digital droplet PCR (ddPCR)-based drop-off assay (Figure 1E). Indel frequencies assayed from zsGreen+ MEFs were 62.3% and 65.2% from gRNAs 1 and 2, respectively (Figure 1F). ddPCR quantification of inversions in bulk genomic DNA showed an average inversion rate of 2.63% (Figure 1G), which corroborates others' work[22–24] showing that deletions (5.74%) occur at roughly twice the frequency of inversions *in vitro*. Our data suggest that the largest barrier to functional deletion *in vitro* is not a lack of editing or inversions, but a lack of simultaneous editing prior to NHEJ repair, resulting in indel formation over a successful deletion.

### Allelic heterogeneity with CRISPR-del *in vivo*

To investigate the frequency of mono- vs. biallelic deletions after CRISPR-del *in vivo*, Ai14/Ai6 mice were co-injected intravenously with 5E12 vg/kg or 1E13 vg/kg AAV8-SaCas9 and AAV8-gRNAs vectors and tissues were collected 14 days later (Figure 3A). Consistent with our Ai14/Ai6 MEF transfection data, livers from treated mice displayed single-positive cell populations that were similar in frequency but with very few double-positive cells (Figure 3B).

Hepatocytes are known to exhibit polyploidy and therefore may contain more than one allele for each reporter gene.[25,26] Using flow cytometry, we could not discern fluorescent populations corresponding to single or multiple activated Ai14-only or Ai6-only alleles and therefore assumed diploid genomes in our calculations (Figure S2). Quantification by flow cytometry after isolation confirmed the allelic heterogeneity noted in tissue sections, with zsGreen-positive cells (3.69% or 4.45%) and tdTomato-positive cells (3.76% or 5.21%) being similar in frequency at doses 5E12 vg/kg and

interrogate the frequency of mono- vs. biallelic deletions after CRISPR-del *in vitro*. Both reporters are in the *Rosa26* safe harbor locus and contain identical upstream floxed STOP cassettes. Thus, the same gRNA sites were used to provide for equal propensity of allelic targeting by CRISPR-del (Figure 1A). Following transfection with plasmids containing SaCas9 and two gRNAs flanking the STOP cassette, we observed equivalent frequencies of MEFs expressing only one fluorophore (3.3% tdTomato and 3.4% zsGreen) and a lower frequency of double-positive (2.4%) cells (Figures 1B and S1A). Overall, there was a CRISPR-del frequency of 5.74% (Figure 1C) with 26.3% of these double-positive ((Figure 1D).

To investigate the editing landscape at the non-expressing allele, MEFs that were single-positive for zsGreen only (zsGreen+/
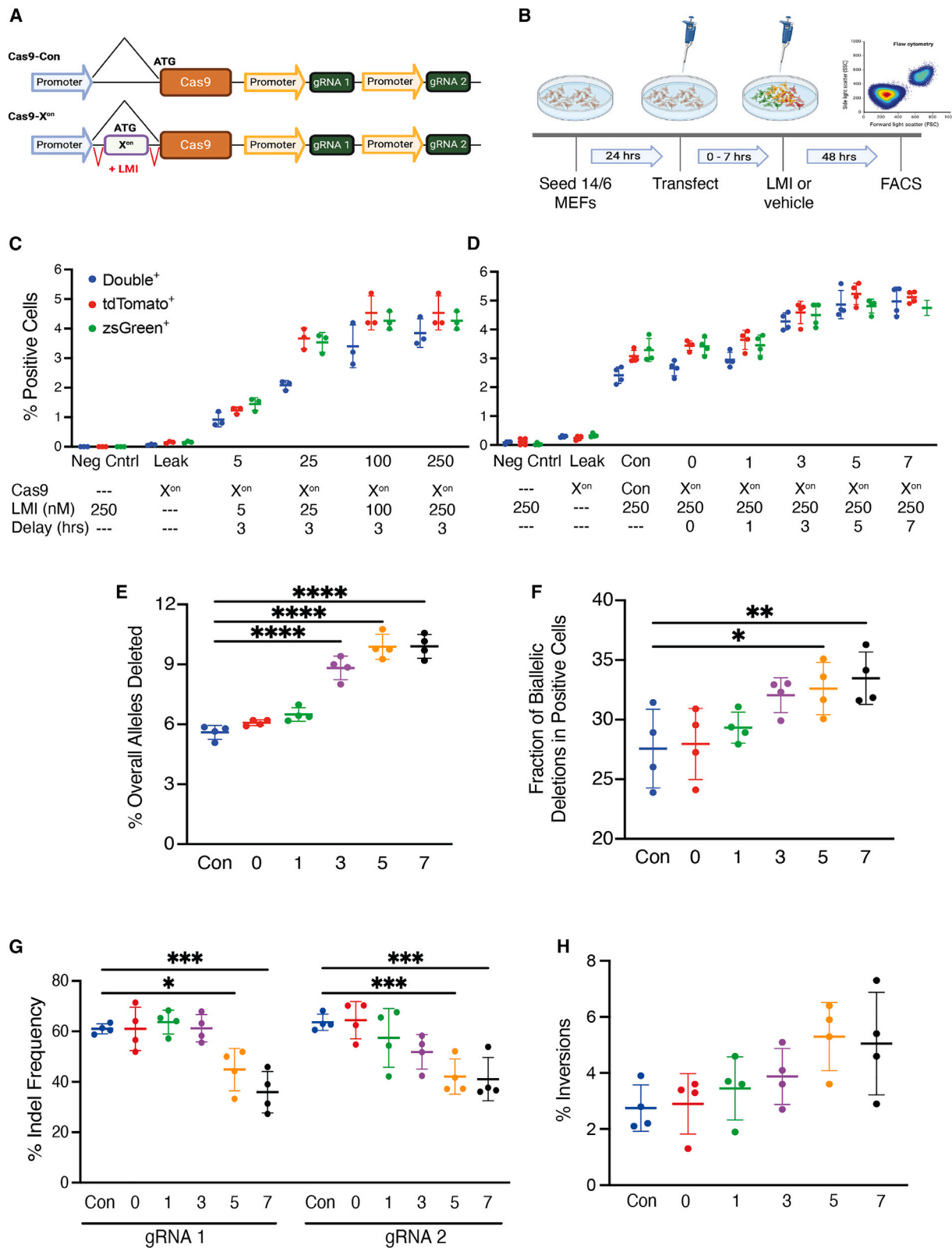
(legend on next page)

1E13 vg/kg, respectively (Figure 3C). Double-positive cells accounted for less than 1% of all hepatocytes at either dose, making up a much lower proportion of the positive cell population at 4.75% and 6.45% (5E12 vg/kg and 1E13 vg/kg) (Figure 4E). Overall, there were 4.09% and 5.51% (5E12 and 1E13) successful deletions (Figure 3D) with single-positive to double-positive deletions at ratios of 20:1 and 15:1 (Figure 3E).

Temporal restriction of CRISPR-Cas9 expression improves CRISPR-del frequency and efficiency *in vitro* and *in vivo*

If the noted high indel frequency at the non-deleted allele gRNA cut sites was due to early expression dynamics following transfection, then temporally restricting Cas9 expression to occur after peak plasmid trafficking may increase the opportunity for simultaneous DSB formation prior to rapid NHEJ repair. To test this, an inducible Cas9 expression cassette was generated using a variant of our previously described X^{on} system.[27] X^{on} utilizes alternative splicing to initiate translation in the presence of the small molecule LMI070. Plasmids were cloned to contain two constitutively expressed gRNAs with either inducible SaCas9 (pSaCas9-X^{on}) or its constitutively expressed counterpart (pSaCas9-Con) (Figure 3A).

Increasing doses of LMI were applied 3 h post-transfection of pSaCas9-X^{on} in Ai14/Ai6 MEFs and the percentage of fluorescent cells at 48 h measured via flow cytometry (Figure 3B). Maximal deletions were observed at 250 nM LMI (Figure 3C). MEFs were then transfected with either pSaCas9-Con or pSaCas9-X^{on}, exposed to 250 nM LMI at varying times, harvested 48 h after initial transfection, and single- and double-positive cells were quantified by flow cytometry. Both mono- and biallelic deletion frequencies increased when translation induction was delayed (Figure 3D), with overall deletion frequency becoming significantly greater at 3, 5, and 7 h (8.8%, 9.8%, and 9.9%) compared with transfection with pSaCas9-Con (5.6%) (Figure 2E). Delayed expression also significantly increased the fraction of cells that were double-positive at 5 and 7 h (32.6% and 33.5%) compared with SaCas9-Con (27.6%) (Figure 3F).

We next sorted, sequenced, and performed ddPCR drop-off analysis at both gRNA cut sites of the tdTomato allele in zsGreen single-positive cells to investigate if the observed improved deletion frequency of X^{on} correlated with reduced indel frequency at non-deleted alleles. pSaCas9-Con transfected cells contained indel frequencies of 61.0% and 63.6% (gRNA1 and gRNA2), while pSaCas9-X^{on} transfected cells showed significantly reduced indel formation with delays of 5 (44.9% at gRNA1 and 42.1% at gRNA2) or 7 h (35.9% at gRNA 1 and 41.1%

at gRNA2) (Figure 3G). Furthermore, we identified that the frequency of inversions increased as deletion frequency increased (Figure 3H). These data support that temporal restriction of Cas9 expression reduces indel formation frequency at gRNA cut sites and improves the opportunity for successful deletions *in vitro* and that inversion, a natural byproduct of simultaneous DSB formation, occurs roughly half as frequently as a successful deletion *in vitro*.

Because of suboptimal induction of Cas9 expression *in vivo* with the cassette used in Ai14/Ai6 MEFs (Figures S3A and S3B), we edited the intron and exon components. Using a dual-luciferase reporter system, there were significant improvements to induction of the new variant, XS3B, compared with the parent variant (XS100 in pSaCas9-X^{on}) post-LMI introduction *in vitro* (Figure S3C), with a concomitant increase in deletion frequency *in vivo* (Figure S3D). AAV8-SaCas9-X^{on}.XS3B (herein noted as XS3B) was then co-injected with constitutively expressed AAV8-gRNAs at a 1:1 ratio into Ai14/Ai6 mice, and LMI dosed either once or three times and cells and tissues analyzed 56 days after AAV delivery (Figure 4A).

Mice that received AAV8-XS3B had increased mono- and biallelic deletions with additional LMI dosing (Figures 4B, 4C, and S4A). Relative to SaCas9-Con (3.0%), overall deletion efficiency was similar for the AAV8-XS3B plus LMI 1x (3.3%) group but was significantly improved in the AAV8-XS3B plus LMI 3x group (7.2%). Notably, the LMI 3x group exhibited over a 5-fold increase in the proportion of double-positive cells compared with SaCas9-Con (7.3% vs. 1.4%) (Figure 4D). These data support that delayed CRISPR/Cas9 expression post-AAV delivery can significantly improve CRISPR-del frequency *in vivo*, particularly in the context of biallelic deletions. To further confirm that observed differences between XS3B and Con groups were not from protein expression variation, liver lysates were assayed by western blot (Figure S4B). AAV-Con-injected mice had 34% more SaCas9 protein than the induced AAV-SX3B groups, suggesting that improvements in X^{on} groups treated with LMI were due to the temporal restriction of transgene expression rather than differences in peak nuclease concentration.

Subsequent ddPCR analysis revealed that both XS3B groups, most notably LMI 3x, averaged significantly fewer indels at gRNA cut sites 1 and 2 (52.0% and 54.3%, respectively) when compared with SaCas9-Con (72.5% and 78.6%, respectively) (Figure 4E). AAV8-XS3B-treated mice given vehicle showed indels of 8.7% and 4.2% (gRNA 1 and gRNA 2), at the non-deleted tdTomato allele (Figure 4E). Thus there is some SaCas9 expression from the XS3B-X^{on} system, which may preclude productive deletions prior to LMI-induced Cas9 expression.

Figure 2. Temporal restriction of CRISPR-Cas9 expression improves CRISPR-del efficiency

(A) Design of transfected transgene cassettes for constitutively on (Cas9-Con) or LMI-inducible SaCas9 (Cas9-X^{on}). (B) Workflow for Ai14/Ai6 MEF transfection and LMI introduction considering varied timepoints. (C) Dose-response curve informing the optimization of X^{on} system for CRISPR-del in Ai14/Ai6 MEFs. (D–F) Summaries of the effect of temporal restriction of Cas9 expression on single- and double-positive cell population size, overall frequency of allelic deletions, and propensity for biallelic deletions. (G) Indel frequency assessed by ddPCR analysis at gRNA cut sites of non-deleted alleles for all groups. (H) Inversion quantifications using ddPCR analysis on bulk genomic DNA from Ai14/Ai6 MEFs. Data in (C)–(H) represent means ± SD, and significance was calculated using an ordinary one-way ANOVA (E, F) or two-way ANOVA (G) followed by Dunnet's post hoc test. *$p < 0.05$, **$p < 0.01$, ***$p < 0.001$, ****$p < 0.0001$.
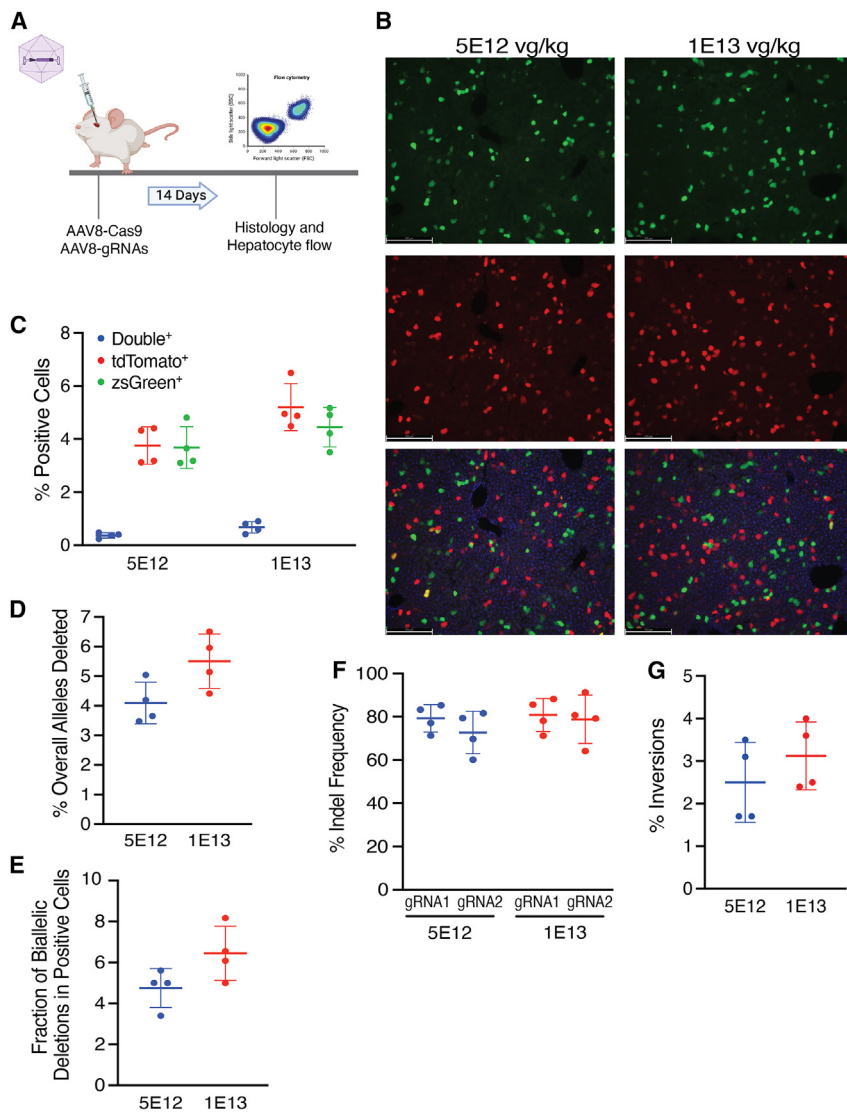
Figure 3. Single-cell resolution of allelic heterogeneity with CRISPR-del *in vivo*

(A) Workflow depicting the delivery of AAV8 vectors encoding SaCas9 and gRNAs at a 1:1 ratio retro-orbitally (systemically) to Ai14/Ai6 mice and the timeline to histological and FACS analysis. (B) Representative histology images of liver sections (40 µm) red, green, and overlay channels. Scale bar is 250 µm. (C–E) Summaries of single- and double-positive cell population size, overall frequency of allelic deletions, and propensity for biallelic deletions, after CRISPR-del *in vivo* using AAV vectors. (F) Indel frequency assessed by ddPCR analysis at gRNA cut sites of non-deleted alleles for both 5E12 vg/kg and 1E13 vg/kg. (G) Quantification of inversions via ddPCR on bulk hepatocyte genomic DNA. Data in (C)–(G) represent means ± SD.

strategy using XS3B-X^{on} may assist in increasing the propensity for deletions over inversions while using AAV.

Temporal restriction of SaCas9-XS3B via XS3B-X^{on} expression impacts anti-Cas9 antibody levels

Constitutive SaCas9 expression may be immunogenic causing clearance of transduced cells.[28–30] To test the impact of delayed expression on antibody titers to AAV-expressed Cas9, we collected sera from treated mice (from Figure 4A) prior to LMI gavage. ELISAs done for Cas9 in sera reached peak levels by d56 for AAV-Con and the AAV-XS3B LMI 1x group (Figure 4G). Interestingly, there were moderate levels of reactivity on d42 of the LMI 3x group that were reduced to not significantly different from baseline by d56. Anti-AAV8 antibodies were not affected, suggesting a potential induction of immune tolerance to the transgene product (Figure S5A).

To investigate if antibody development was coupled to clearance of transduced hepatocytes ddPCR was used to quantify SaCas9 transgenes per diploid genome in bulk sorted hepatocytes. There were no significant differences of viral genomes per diploid genome (vg/dpge) between groups (Figure S5A).

Lipid nanoparticle delivery of CRISPR-del machinery improves deletion frequency *in vivo*

Unlike AAVs, lipid nanoparticles (LNPs) can deliver an immediate pulse of high transgene expression, which we hypothesize may greatly improve the opportunity for simultaneous DSBs and subsequent successful CRISPR-del. LNPs additionally can lack intrinsic

To investigate the editing landscape in these groups, we used ddPCR to evaluate the frequency of inversions found within hepatocytes. Expectedly, inversion rates increased as deletion frequency increased. This was observed with the Con and 1x groups, as they averaged similar rates of both overall deletions (3.0% and 3.3%, respectively) as well as inversions (2.3% and 1.8%, respectively) (Figure 4F). In contrast, the LMI 3x group averaged more deletions (7.2%) as well as inversions (3.7%). Compared with the traditional constitutively expressed SaCas9-Con, the XS3B-X^{on} approach moderately skews toward a productive deletion rather than an inversion. This is exemplified in our 1x and 3x groups, as they averaged 1.83 and 1.95 deletions per inversion, respectively. This contrasts the constitutively expressed group, which averaged 1.3 deletions per inversion. These data suggest that inversions are a natural byproduct of CRISPR-del, but that this restricted expression
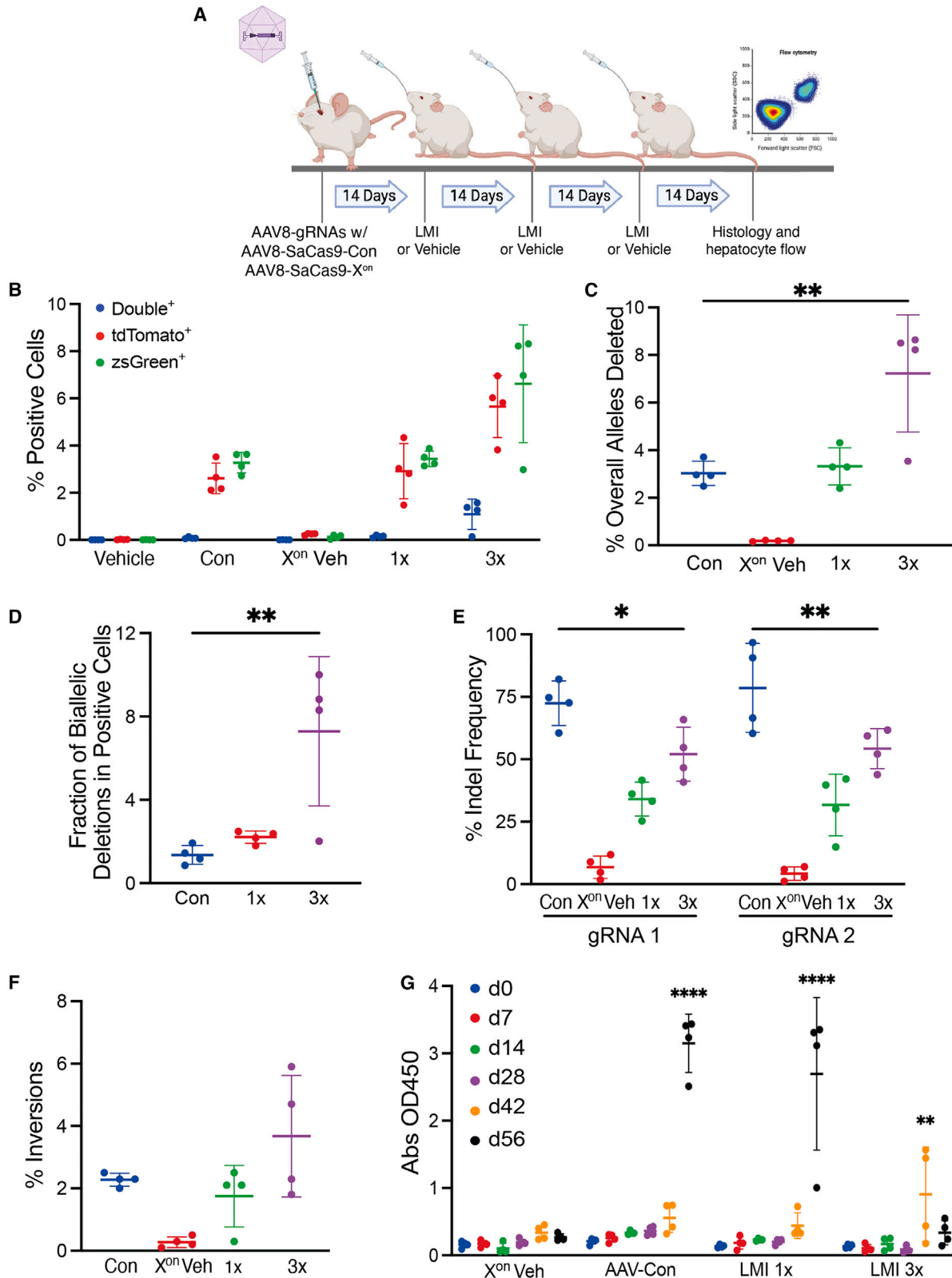
immunogenicity as a delivery vehicle,[4,31] in contrast to AAV, which cannot be re-dosed systemically *in vivo*.[32–34] As AAV8-SaCas9-X[on] showed stepwise improvements in CRISPR-del success with each introduction of LMI (Figure 4C), we sought to also investigate a similar additive potential of LNPs.

To evaluate single- and dual-injections of LNPs on CRISPR-del efficiency, we injected Ai14/Ai6 mice intravenously with hepatocyte-tropic LNPs (Table S1; Figure S7) containing a 2:1:1 ratio of SpCas9 mRNA, gRNA1, and gRNA2, at 2 or 4 mg/kg (Figure 5A). As we observed stepwise increases with each LMI-induced burst in our X[on] experiments (Figures 4B and S3B), we then repeated LNP injections 14 days after with either empty or full LNPs and harvested tissues 14 days post-second injection for hepatocyte sorting and flow cytometry analysis (Figure 5A). Single-dose groups displayed a notable dose-dependent increase in the allelic heterogeneity between 2 mg/kg and 4 mg/kg, with their dual-dose counterparts exhibiting minimal increases in all positive cell populations (Figure 5B). The single-injection low-dose-treated animals displayed monoallelic deletion frequencies roughly twice that of AAV-Con, with 4.78% and 5.70% zsGreen- or tdTomato-positive cells, and substantially higher biallelic deletions with 4.78% double-positive cells (Figure 5C). A single repeat injection of full LNP in the low-dose group roughly doubled the presence of single-positive cells with 8.80% and 9.63% zsGreen or tdTomato but showed modest improvements to double-positive cells at 6.97%. In contrast, the singly injected high-dose-treated animals averaged 11.71% and 12.32% zsGreen- or tdTomato-positive cells, while the double-positive population in this high-dose group was 33.41% of all hepatocytes collected (Figure 5C). Mice that received two 4 mg/kg injections showed no statistical increase in single- or double-positive cell frequencies over their singly dosed counterparts, with 13.06% and 13.36% zsGreen or tdTomato single-positive cells and 36.65% double-positive cells.

Overall, redosing of LNPs had a nonsignificant improvement on overall deletion frequency for the low-dose (11.18% for 1x and 16.18% for 2x) or the high-dose groups (45.42% for 1x and 50.00% for 2x) (Figure 5D). Furthermore, the fraction of double-positive cells that made up the overall positive cell population were not significantly improved after repeat dosing for either the low-dose (27.12% for 1x and 27.60% for 2x) or high-dose groups (57.92% for 1x and 57.81% for 2x) (Figure 5E). Analysis of indel frequency via ddPCR on sorted zsGreen-only cells revealed dose-dependent increases in indels of singly dosed groups for both gRNA1 (35.5% and 69.3% for 2 or 4 mg/kg) and gRNA2 (38.7% and 72.0% for 2 or 4 mg/kg) (Figure 5F). Compared with singly dosed animals, repeat dosing of editing cargo significantly increased indel frequency at both gRNA cut sites for the low-dose group (76.7% at gRNA1 and 69.5% at gRNA2), but did not significantly increase indel frequency at either gRNA cut site for the repeated high-dose group (81.5% at gRNA 1 and 83.6% at gRNA2). Redosing did not alter inversion frequencies (Figure 5G).

These data emphasize that repeat dosing with the same CRISPR-del components does not significantly increase deletion nor inversion frequency but does increase the frequency of indels at gRNA cut sites of non-activated alleles. Overall, the LNP data support that rapid high expression of CRISPR-Cas9 nucleases are essential for successful deletions, but that residual indel scars preclude the utility of repeat doses.

Next, sera from injected mice were subjected to anti-SpCas9 ELISAs (Figure 5H). Notably, we observed no increase in reactivity over time to SpCas9 antigen, suggesting no notable immunogenicity despite re-exposure. These data support the potential safety of repeat dosing of LNPs for CRISPR-Cas gene editing in liver.

DISCUSSION

Efforts to characterize CRISPR-del have historically relied on cell or animal models expressing a single fluorophore. As shown in prior work by us and others, systems like the Ai14 mouse model allow visualization of CRISPR-del with single-cell resolution.[19] These systems have enabled work to improve CRISPR-del by engineered CRISPR-Cas9 variants, non-viral delivery technologies, and transient NHEJ DNA repair inhibition. However, single fluorophore reporter models cannot empirically discern between mono- vs. biallelic deletions and are therefore blind to the allelic heterogeneity of editing approaches like CRISPR-del, which is relevant to human disease application. Here, we used Ai14/Ai6 mice and MEFs derived from them as deletion-dependent dual-color reporter cell and mouse model systems for their ability to sensitively discern mono- vs. biallelic deletions on a single-cell level.

The frequency of successful CRISPR-del events has historically been infrequent despite high dosing *in vivo*, further corroborated by our data. Prior *in vitro* research suggested rapid NHEJ repair as a major barrier to productive deletions,[16,17] which our data support. NHEJ repair, and therefore indel formation, can occur almost immediately after nuclease activity.[35] We found that limiting the window of CRISPR-Cas9 expression increased simultaneous DSB formation. With pSaCas9-X[on], overall deletion frequency improved *in vitro* with each hour of delayed expression post-transfection, emphasizing the importance of preventing low levels of transgene expression prior to peak expression from plasmids.

Figure 4. Temporal restriction of CRISPR-del via AAV-XS3B improves biallelic deletion frequencies and reduces indel installment *in vivo*
(A) Workflow depicting the route of administration for AAV vectors, timeline for gavage of LMI or vehicle, and endpoint collection of tissues for histology and flow sorting. (B–D) Summaries of single- and double-positive cell population size, overall frequency of allelic deletions, and propensity for biallelic deletions after temporal restriction of AAV-delivered SaCas9. (E) Indel frequencies assessed by ddPCR analysis at gRNA cut sites of non-deleted alleles for all groups. (F) Quantification of inversions found in bulk hepatocyte genomic DNA. (G) Anti-SaCas9 antibodies measured at baseline (day 0) through day 56 post injection. Data in (B–F) represent means ± SD, and significance was calculated using an ordinary one-way ANOVA (C and D) or two-way ANOVA (E) followed by Dunnet's post hoc test. *p < 0.05, **p < 0.01, ****p < 0.0001.
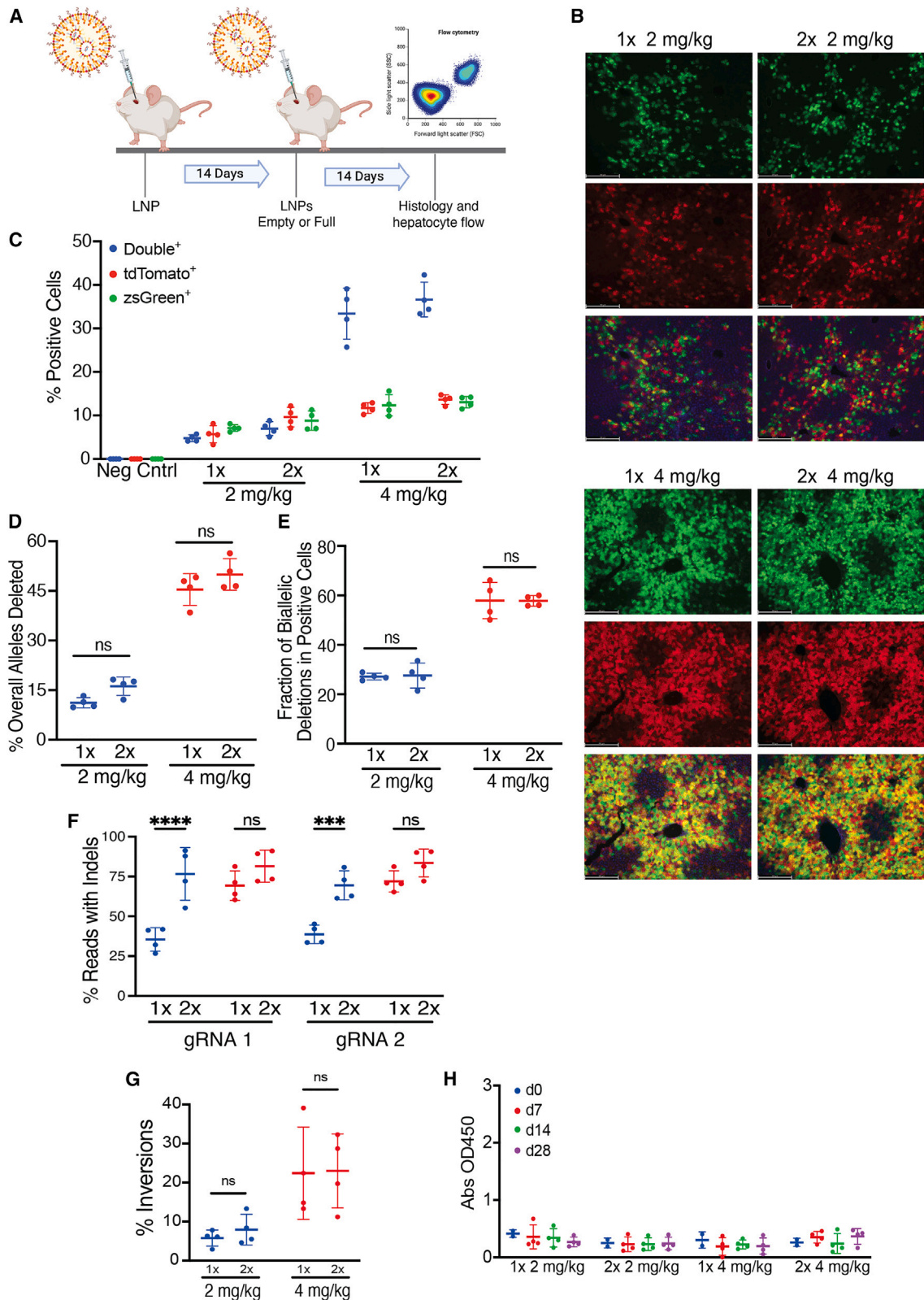
In vitro, transfections reach maximum expression in hours,[36–38] while AAV-delivered transgenes express at low levels rapidly after *in vivo* delivery but peak after several weeks.[39,40] Low expression levels can therefore induce DSBs at single gRNA sites non-simultaneously, resulting in indel scar formation and prevention of target deletion. The importance of avoiding even minimal levels of expression prior to peak expression was emphasized in our vehicle-treated AAV-XS3B group. Tissues from this group displayed measurable indel formation presumably from low levels of transgene leakage detectable in this sensitive reporter mouse, further supporting the need for a delivery technology capable of circumventing even low levels of transgene expression prior to induction of high expression. With optimal dosing, however, AAV-XS3B resulted in a biallelic deletion frequency of 1.09% of all hepatocytes, a rate over 13-fold higher than when using its constitutively expressed counterpart AAV-Con (0.08%).

Whereas AAV transgene expression peaks 2–3 weeks post-transduction, LNPs have rapid maximum expression *in vivo*.[41,42] Notably, our singly injected high-dose LNP-treated mice had a robust overall deletion frequency and a biallelic deletion frequency that out-numbered monoallelic deletions. Repeating LNP delivery had minimal impact although the low-dose group had a greater improvement from the second dose, presumably from less indel formation at gRNA cut sites This additionally highlights the importance of maximal Cas9 intracellular concentration, in conjunction with a limited expression window, as the expression kinetics between 2 mg/kg and 4 mg/kg should be similar, yet the deletion frequencies were vastly different.

Here, we used different CRISPR-Cas orthologs for AAV (SaCas9) and LNP (SpCas9) experiments. Due to AAV transgene size constraints (roughly 4.6 kb maximum), studying the effect of X^{on}-mediated transgene restriction on CRISPR-del required SaCas9 rather than SpCas9. Also, unlike SpCas9 mRNA, commercially available modified mRNA for SaCas9 was not available at the time of our study. Interpretation of CRISPR-del frequency between the two technologies (AAV and LNPs) should consider that SpCas9 is a single-turnover enzyme that continues to bind to PAM-distal DNA for up to 24 h, while SaCas9 is a multiple-turnover enzyme that releases target DNA within hours after cleavage. This subtle difference could result in varied degrees of steric blocking of DNA repair machinery that may otherwise rapidly repair broken ends.

The threshold of deletion frequency for therapeutic relevancy of CRISPR-del varies based on the disease. HIV, for example, may require a near 100% deletion efficacy to prevent reactivation of latent integrated proviruses. In contrast, reactivation of the fetal hemoglobin gene via CRISPR-del of the BCL11A enhancer in only 20% of erythrocytes is suggested to drastically improve disease symptoms of sickle-cell anemia in humans.[43,44] Our data, while quantified in the liver, demonstrated 45% overall deletion frequency with a single injection of highly concentrated LNPs. This deletion frequency suggests that reaching therapeutic thresholds for HIV or sickle-cell anemia is promising, as LNPs efficiently transfect CD4+ T-cells[45] (the main cellular reservoir for HIV) and hematopoietic stem cells[46] (progenitors of erythrocytes). Use of the Ai14/Ai6 model will allow for the optimization of LNP-based delivery of CRISPR-del components. Our data suggest that a 20% deletion threshold for sickle-cell anemia may be possible with a single dose of LNPs, whereas HIV therapy may require repeat dosing with gRNAs not used previously. The increase from single- and double-positive hepatocyte populations in conjunction with increased indel frequencies at gRNA cut sites after subsequent LNP dosing suggests the lack of clearance of hepatocytes from CRISPR-Cas9 or LNP immunogenicity. This is further corroborated by assays for anti-Cas9, where we found no significant presence of anti-SpCas9 antibodies despite repeat injections. It will be important to assess longer time points to determine if the low anti-transgene response is maintained.

Here, we present differences in the range of biallelic deletion frequency resulting from CRISPR-del via different delivery modalities. These data will inform CRISPR-del approaches for all phenotypes, but more specifically those that require biallelic deletions such as autosomal recessive diseases,[47,48] or where mutant allele-specific gRNAs are not readily available,[49] or in situations where the targeted sequence for excision is located multiple times within the genome.[50–52]

While our data demonstrate variabilities in mono- and biallelic deletion frequencies dependent on delivery modality, others showed improvements via chemical inhibition of essential NHEJ repair proteins.[16,17] It is possible that coupling NHEJ inhibition with restricted nuclease expression could further improve overall and/or biallelic deletion frequencies. Assessing the impact of transient NHEJ inhibition on CRISPR-del *in vivo*, however, would be best assessed by LNP delivery or AAV-X^{on} as AAV episomal establishment utilizes NHEJ repair protein machinery.[53]

Temporal restriction of CRISPR-Cas9 may additionally improve the safety profile of CRISPR-del therapeutic approaches. In terms of three major concerns of AAV-delivered CRISPR-Cas9 *in vivo*: transgene immunogenicity, off-target effects, and AAV-genome integration may each be improved by temporal restriction of nuclease

Figure 5. Lipid nanoparticle delivery of CRISPR-del machinery further improves deletion frequency *in vivo*

(A) Workflow and timeline depicting the route of administration for LNP injections and endpoint collection of tissues for histology and FACS sorting. (B) Histology of one mouse from each group depicting liver sections (40 μm) with green, red, and overlay channels. (C–E) Summaries of single- and double-positive cell populations, overall frequency of allelic deletions, and propensity for biallelic deletions after one or two infusions of LNP-SpCas9+gRNAs. (F) Indel frequency calculations after ddPCR analysis at gRNA cut sites of non-deleted alleles for all groups. (G) Quantification of inversions via ddPCR on hepatocyte genomic DNA. (H) Quantitation of anti-SpCas9 antibodies in mice following LNP nanoparticle delivery. Days 0 (baseline) to 28 days post treatment are shown. Data in (C–G) represent means ± SD and significance was calculated using a two-way ANOVA followed by Dunnet's post hoc test. ***p < 0.001, ****p < 0.0001.

expression.[54–56] Approaches to limit expression of nucleases include self-deleting transgene constructs for AAV delivery wherein expression is terminated after intended editing has occurred.[57,58] While humans may have pre-existing immunity to various CRISPR-Cas9 proteins,[29] whether this is problematic for therapeutic application remains untested. Nonetheless, prolonged expression of bacterial proteins could be problematic, making either the X^{on} system or LNP delivery desirable. Using X^{on} there was a measurable increase in single- and double-positive cells with each biweekly introduction of the LMI on-switch, suggesting that transduced cells were not cleared by the immune system despite the re-introduction of CRISPR-Cas9 antigen. Interestingly, there were reduced anti-transgene responses with the X^{on} system with redosing that did not occur upon a single induction. We hypothesize that this approach may be mimicking that of immune tolerance induction (ITI) utilized widely by medical professions aiming to quell antibody responses to infused therapeutic proteins, such as Factor VIII in the context of hemophilia A patients. It is possible that early low-level expression in the absence of drug (Figure 4E) allowed the priming of tolerance induced after LMI introduction and may in turn be beneficial if using X^{on} *in vivo* for repeated expression in a therapeutic setting. This would be in contrast to AAV-Con, which induces a strong antibody response to the Cas9 protein.[4,28,59,60] Furthermore, constitutive nuclease expression from AAVs has revealed full-length and fragment integration.[15,61] It will be interesting to test in further work if X^{on}-restricted expression reduces unwanted rearrangements or integration in addition to improving the frequencies of CRISPR-del.

In summary, we characterized the genomic outcomes of CRISPR-del *in vitro* and in liver using either constitutive or delayed expression post transgene delivery, or via LNP. The Ai14/Ai6 model provided insights into the resultant allelic heterogeneity after CRISPR-del in single cells, emphasizing the importance of simultaneous DSB formation prior to NHEJ repair and indel formation. Furthermore, we present two methods of restricting Cas9 expression that in turn increased the frequency of mono- and biallelic deletions. These approaches may help us further define the relationship between CRISPR-del and endogenous DNA repair.

MATERIALS AND METHODS

Animals

All animal procedures were previously approved by The Children's Hospital of Philadelphia Institutional Animal Care and Use Committee. Ai6 (B6.Cg-Gt(ROSA)26Sor$^{tm6(CAG-zsGreen1)Hze}$/J, Stock No: #007906) and Ai14 (B6.Cg-Gt(ROSA)26Sor$^{tm14(CAG-tdTomato)Hze}$/J, Stock No: #007914) were obtained from Jackson Laboratories. Ai14 and Ai6 mice were crossed to generate compound heterozygous Ai14/Ai6 mice, with each containing one copy of a tdTomato (Ai14) floxed allele and one copy of a zsGreen (Ai6) floxed allele. Offspring from these crosses were confirmed for genotype using PCR primers and protocols available on the Jackson Laboratory website. Mice were housed in a temperature-controlled, enriched environment on a 12-h light/dark cycle. Food and water were provided libitum. All studies were performed with adult (>5 weeks old), male mice.

AAV vectors

All AAV8 vectors (AAV8-SaCas9, AAV8-SaROSAgRNAs, AAV8-SaCas9-Con, AAV8-SaCas9-X^{on}, and AAV8-SaCas9-XS3B3) were manufactured by the Children's Hospital of Philadelphia Research Vector Core. Vector titer was determined by ddPCR and recorded in gene copies (GC) per milliliters. The AAV8-ROSA-SagRNAs vector contained the following gRNA sequences: 5′-CTCTAGAGTCG CAGATCCTC-3′ and 5′-ACGAAGTTATATTAAGGGTT-3′.

Nucleic acids and lipid nanoparticles

SpCas9 mRNA was purchased from TriLink Biotechnologies (CleanCap Cas9 mRNA, L-7606). Chemically end-modified synthetic gRNAs (Synthego, Redwood City, CA) contained the following sequences: 5′-AAAGAATTGATTTGATACCG-3′ and 5′-GTATGC TATACGAAGTTATT-3′. Nucleic acids were mixed at a ratio of 2:1:1 (mRNA:gRNA1:gRNA2) prior to encapsulation by lipid nanoparticles (LNPs). Lipids including SM-102, DSPC, cholesterol, and DMG-PEG2K were diluted in ethanol at a 50:10:38.5:1.5 mol percent ratio and mixed with RNA (sodium acetate, pH 4) at an N:P ratio of 5.8 using an in-house T-mixer. Mixing parameters included a flow rate ratio of 1:3, a total flow rate of 15 mL/min. LNPs were immediately dialyzed against 1X PBS for 4 h (10 kDa MWCO) to remove ethanol and reach target pH. LNPs were then concentrated, filter sterilized, and frozen using a proprietary cryoprotectant buffer composition (pH 7.45). The hydrodynamic size, polydispersity index (PdI), and surface charge (zeta potential) of the formulated LNPs were determined using a Zetasizer Nano ZS90 (Malvern Instruments) (Table S1). The morphology of LNPs was characterized by cryo-EM (Titan Krios, Thermo Fisher) with a K3 Bioquantum (Gatan). RNA encapsulation efficiency and the apparent pKa of LNPs were determined using a modified Quant-iT RiboGreen RNA assay (Invitrogen) and the 6-(p-toluidinyl)naphthalene-2-sulfonic acid assay, respectively.[62] Endotoxin levels were examined by the chromogenic endpoint Limulus amebocyte lysate (LAL). All LNPs were stored at −80°C until use, and the endotoxin levels were below detection limits.

Mouse procedures and histology

For systemic retro-orbital AAV and LNP injections, mice were anesthetized with isoflurane. The right eye was numbed with drops of Proparacaine hydrochloride Ophthalmic Solution, USP 0.5%, prior to retro-orbital injection. Injectant was diluted up to a volume of 200 μL using vector dilution buffer (0.01 M sodium phosphate dibasic, 0.18 M sodium chloride, and 0.001% Pluronic F-68 dialysis buffer, pH = 7.4) according to the desired dose (2 mg/kg or 4 mg/kg for LNPs, and 5E12 vg/kg, 1E13 vg/kg or 1.75E13 vg/kg for AAV). Vehicle-injected mice received 200 μL of vector dilution buffer alone. The entire volume was quickly injected into the retro-orbital venous sinus behind the right eye using a BD U-100 insulin syringe (Becton Dickinson). For gavage, LMI (LMI070, MedChemExpress, HY-19620) was diluted in a 1:1 mixture of 1% methylcellulose and 1% Tween-80 to a concentration of 5 mg/mL. Mice were dosed with LMI at 50 mg/kg. For perfusions and tissue collection, mice were anesthetized with isoflurane and perfused with 20 mL of ice-cold PBS. Heart, lung, liver, kidney, and spleen were collected from all mice

and post-fixed in 4% PFA with a 24-h incubation at 4°C and then cryoprotected with a 72-h incubation at 4°C in a 30% sucrose solution (in PBS). After cryoprotection, organs were stored frozen at −80°C. Cryoprotected Ai14/Ai6 mouse tissues were sectioned on a freezing microtome at 40 μm. Tissues were rinsed with PBS, stained for nuclei with a 1:5,000 dilution of Hoechst 33528 (in PBS), rinsed again in PBS, and then mounted with Fluoro-Gel (Electron Microscopy Sciences) and coverslipped. Mounted sections were imaged with a LEICA DM6000 B epifluorescence microscope using a ×10 dry objective.

Hepatocyte isolation and flow cytometry

After perfusion of mice, as mentioned above, livers were minced with a razor blade and enzymatically digested for 2 h at 37°C with shaking (digestion solution: 3 mM CaCl2, 200 units/mL Collagenase IV, and 1.5% bovine serum albumin [BSA] in Hank's balanced salt solution [HBSS]). The final hepatocyte suspension was passed through a 70-μm filter and rinsed to assist in straining cells through the filter (washing buffer: 1.5% BSA in HBSS). Cells were pelleted by centrifugation ($110 \times g$) and resuspended in FACS buffer (0.5% BSA, EDTA (2 mM) in PBS), and counted using Trypan Blue (1:10 dilution) to determine the total count of live cells. Cells were aliquoted and stained with 0.29 μg/μL of a hepatocyte-specific primary (Rabbit anti-Mouse ASGR1, Proteintech, 11739-1-AP) or immunoglobulin (Ig)G control primary (Rabbit IgG, Vector Laboratories, I-1000-5) for 30 min at room temperature. Cells were pelleted at $110 \times g$ and rinsed twice with FACS buffer. Cells were then resuspended and stained with secondary (donkey anti-rabbit IgG H + L, Alexa Fluor 647, Thermo Fisher, A32733) at a 1:400 dilution for 15 min at room temperature. Cells were rinsed three times and resuspended in 1 mL FACS buffer. Flow cytometric analysis and sorting was performed on an FACS Aria Sorter (BD Biosciences). Suspensions were gated for cells, singlets, and hepatocytes (APC-A) (except for *in vitro* MEFs work) and then gates for tdTomato (PE) and ZsGreen (FITC) were established on non-edited controls (Figure S2). Data were analyzed using FlowJo 10.8.2 software (FlowJo LLC).

Evaluation of indel frequency at gRNA cut sites

Genomic DNA was isolated from zsGreen-only hepatocytes using the QIamp mini kit (Qiagen). Evaluation of indel frequency in Cas9-treated groups was performed using a ddPCR drop-off assay. For SaCas9 gRNA 1, primers used were Fwd 5′- AGGAACTTCGT CGACATTTAAATCA-3′ and Rev 5′-CTACAAATGTGGTATGGC TGATTATG-3′. For SpCas9 gRNA 1, primers used were Fwd 5′- CC TACAGCTCCTGGGCAA-3′ and Rev 5′-TTATTCATCGCGAATA ACTTCGT-3′. For amplification of the downstream (gRNA 2) cut sites for both SaCas9 and SpCas9, the following primers were used: Fwd 5′-ATCATGTCTGGATCCCCATCAA-3′ and Rev 5′-TC GCCCTTGCTCACCATGGT-3′. Reference (Ref) and drop-off (DO) probes were as follows: SaCas9_Ref_gRNA1 = 5′-TATGCTA TACGAAGTTATTCGCGAT-3′

SaCas9_DO_gRNA1 = 5′-CGACTCTAGAGGATCTGCGACTC–3′, SpCas9_Ref_gRNA1 = 5′-CTCTAGAAAGTATAGGAACTTCGTC GAC-3′

SpCas9_DO_gRNA1 = 5′-TTTGATACCGCGGGCCCTAA-3′

SaRef_SpDO_gRNA2 = 5′-CTATACGAAGTTATTAGGTCCCTC GACCT.

SaDO_SpRef_gRNA2 = 5′-CTGATCCGGAACCCTTAATATAACT TCGTAT-3′

All probes were ordered in both of the following versions: (1) 5′ 6-FAM/ZEN/3′ IBFQ and (2) 5′ Hex/ZEN/3′ IBFQ, and correct combinations were utilized for each ddPCR reaction to ensure the reference and drop-off probes were of different fluorescence probe signal. The PCR reaction cycle conditions were 95°C for 10 min (95°C 10 for seconds, 60°C for 30 s) × 39, 95°C for 10 min, 4°C hold. To quantify percent indel frequencies, the total number of singly fluorescent droplets (reference probe binding only) were divided by the total number of doubly fluorescent droplets (reference and drop-off probe binding) × 100.

Western blot

Protein lysates were obtained from mouse livers using RIPA buffer as a lysing reagent, and concentration was measured via Bradford protein assay according to the manufacturer's instructions (Bio-Rad). Twenty micrograms of protein was loaded into a 4%–20% Citeron TGX gel and run for 1 h at 110 V. Proteins were then transferred to PVD membrane using the Turbo-Blot Turbo Transfer system (Bio-Rad), and subsequently blocked with 5% milk in TBS-T for 2 h at room temperature. Primary antibodies for detecting HA-tagged SaCas9 (Rabbit mAb, C29F4, Cell Signaling Tech.) and αTubulin (Mouse mAB, T5168, Millipore Sigma) were diluted 1:2,000 and 1:10,000, respectively, and added to the membrane overnight at 4°C on a shaker. The membrane was then washed 3x at 10-min intervals with TBS-T and HRP-conjugated goat-anti-Rabbit and goat-anti-Mouse secondaries (diluted 1:5,000) were added for 2 h at room temperature. Membranes were washed 3x at 10-min intervals with TBS-T and detection reagent was added for 5 min (Cytiva's Amersham ECL). Membranes were imaged for chemiluminescence intensity and quantified for Gray Mean Value via ImageJ software. To quantify differences in groups, the ratio of HA-SaCas9 (experimental) to αTubulin (loading control) was calculated for each lane. Listed values (Figure S4B) depict the total mean ratio of each group.

Cell culture

MEFs were isolated from Ai14/Ai6 compound heterozygous embryos using a protocol described in Jozefczuk et al.[63] The protocol was followed through the first section and the steps after this were not performed. Briefly, a pregnant homozygous Ai6 mouse was euthanized at day 14 post-coitum (with a homozygous Ai14 male). The uterine horns were dissected for isolation of embryos. Heads and red organs were extracted, and the remaining tissues were minced and trypsinized. Trypsin was then neutralized with the addition of MEF culture media (45 mL of DMEM, 50 mL of FBS, 5 mL of 200 mM L-glutamine, and 5 mL of penicillin-streptomycin). The cells were then plated onto coated cell culture plates and allowed to expand.

In vitro transfection and drug treatment

Ai14/Ai6 MEFs were seeded onto uncoated six-well plates. Cells were transfected at 70%–80% confluence using Lipofectamine 3000 (Thermo Fisher) according to manufacturer's protocols. Media was changed 24 h later and cells were maintained for 72 h total after transfection. MEFs were then imaged with an EVOS FL Cell Imaging System (Thermo Fisher).

The Cre-encoding plasmid, pENN.AAV.CMVs.PI.Cre.rBG, was obtained from Addgene (Addgene plasmid #105537; http://n2t.net/addgene:105537; RRID:Addgene_105537).

For *in vitro* experiments using LMI: MEFs were transfected as aforementioned and treated with designated concentrations of LMI (LMI070, MedChemExpress, HY-101792A) diluted in DMSO at designated time points post-transfection. Cell culture media was changed 24 h after introduction of LMI and cells were lifted and prepared for flow cytometry 72 h after initial transfection.

ELISAs

Ninety-six-well plates were coated overnight at 4°C with 100 μL of either SaCas9 or SpCas9 at 1 μg/mL in PBS. Plates were washed with 200 μL of 0.05% PBS-T three times and coated in 5% milk in PBS for 1 h at 37°C then dumped. Samples were diluted 1:20 or 1:50 in 5% milk in PBS for at least 30 min and added to the plate for 1 h at 37°C. Plates were dumped and washed five times with 200 μL of 0.05% PBS-T. Donkey anti-mouse HRP antibody was diluted 1:2,000 in 5% milk in PBS and 100 μL was added to the plates for 1 h at 37°C. Plates were dumped and washed 10 times with 0.05% PBS-T. Fifty microliters of TMB start reaction was added to each well and allowed to develop for 10 min. Fifty microliters of TMB stop solution was then added to wells and absorbance values were read at 450 nm.

Figure generation

The graphical abstract and following figures were created with the assistance of biorender.com: Figures 1A, 1E, 2A, 2B, 3A, 4A, 5A, and S3A.

Statistical analysis

Statistical analyses were performed using GraphPad Prism v.9.1.2 software. Data were analyzed using one-way ANOVA or two-way ANOVA followed by a Dunnet's post hoc test. Statistical significance was considered when $p < 0.05$. All results are shown as mean ± SEM.

DATA AND CODE AVAILABILITY

The data that support the findings of this study are available from the corresponding author upon reasonable request.

SUPPLEMENTAL INFORMATION

Supplemental information can be found online at https://doi.org/10.1016/j.omtn.2024.102172.

REFERENCES

1. Shin, J.W., Hong, E.P., Park, S.S., Choi, D.E., Zeng, S., Chen, R.Z., and Lee, J.M. (2022). PAM-altering SNP-based allele-specific CRISPR-Cas9 therapeutic strategies for Huntington's disease. Mol. Ther. Methods Clin. Dev. 26, 547–561.

2. Herskovitz, J., Hasan, M., Patel, M., Blomberg, W.R., Cohen, J.D., Machhi, J., Shahjin, F., Mosley, R.L., McMillan, J., Kevadiya, B.D., and Gendelman, H.E. (2021). CRISPR-Cas9 Mediated Exonic Disruption for HIV-1 Elimination. EBioMedicine 73, 103678.

3. Xiang, X., Zhao, X., Pan, X., Dong, Z., Yu, J., Li, S., Liang, X., Han, P., Qu, K., Jensen, J.B., et al. (2021). Efficient correction of Duchenne muscular dystrophy mutations by SpCas9 and dual gRNAs. Mol. Ther. Nucleic Acids 24, 403–415.

4. Kenjo, E., Hozumi, H., Makita, Y., Iwabuchi, K.A., Fujimoto, N., Matsumoto, S., Kimura, M., Amano, Y., Ifuku, M., Naoe, Y., et al. (2021). Low immunogenicity of LNP allows repeated administrations of CRISPR-Cas9 mRNA into skeletal muscle in mice. Nat. Commun. 12, 7101.

5. Cong, L., Ran, F.A., Cox, D., Lin, S., Barretto, R., Habib, N., Hsu, P.D., Wu, X., Jiang, W., Marraffini, L.A., and Zhang, F. (2013). Multiplex genome engineering using CRISPR/Cas systems. Science 339, 819–823.

6. Han, J., Zhang, J., Chen, L., Shen, B., Zhou, J., Hu, B., Du, Y., Tate, P.H., Huang, X., and Zhang, W. (2014). Efficient in vivo deletion of a large imprinted lncRNA by CRISPR/Cas9. RNA Biol. 11, 829–835.

7. Yang, H., Wang, H., Shivalila, C.S., Cheng, A.W., Shi, L., and Jaenisch, R. (2013). One-step generation of mice carrying reporter and conditional alleles by CRISPR/Cas-mediated genome engineering. Cell 154, 1370–1379.

8. Lee, H.J., Kim, E., and Kim, J.S. (2010). Targeted chromosomal deletions in human cells using zinc finger nucleases. Genome Res. 20, 81–89.

9. Fang, L., Monteys, A.M., Dürr, A., Keiser, M., Cheng, C., Harapanahalli, A., Gonzalez-Alegre, P., Davidson, B.L., and Wang, K. (2023). Haplotyping SNPs for allele-specific gene editing of the expanded huntingtin allele using long-read sequencing. HGG Adv. 4, 100146.

10. Monteys, A.M., Ebanks, S.A., Keiser, M.S., and Davidson, B.L. (2017). CRISPR/Cas9 Editing of the Mutant Huntingtin Allele In Vitro and In Vivo. Mol. Ther. 25, 12–23.

11. Yin, C., Zhang, T., Qu, X., Zhang, Y., Putatunda, R., Xiao, X., Li, F., Xiao, W., Zhao, H., Dai, S., et al. (2017). In Vivo Excision of HIV-1 Provirus by saCas9 and Multiplex Single-Guide RNAs in Animal Models. Mol. Ther. 25, 1168–1186.

12. Canver, M.C., Bauer, D.E., Dass, A., Yien, Y.Y., Chung, J., Masuda, T., Maeda, T., Paw, B.H., and Orkin, S.H. (2014). Characterization of genomic deletion efficiency mediated by clustered regularly interspaced short palindromic repeats (CRISPR)/Cas9 nuclease system in mammalian cells. J. Biol. Chem. 289, 21312–21324.

13. Park, S.H., Cao, M., Pan, Y., Davis, T.H., Saxena, L., Deshmukh, H., Fu, Y., Treangen, T., Sheehan, V.A., and Bao, G. (2022). Comprehensive analysis and accurate quantification of unintended large gene modifications induced by CRISPR-Cas9 gene editing. Sci. Adv. 8, eabo7676.

14. Wen, W., Quan, Z.J., Li, S.A., Yang, Z.X., Fu, Y.W., Zhang, F., Li, G.H., Zhao, M., Yin, M.D., Xu, J., et al. (2021). Effective control of large deletions after double-strand breaks by homology-directed repair and dsODN insertion. Genome Biol. 22, 236.

15. Simpson, B.P., Yrigollen, C.M., Izda, A., and Davidson, B.L. (2023). Targeted long-read sequencing captures CRISPR editing and AAV integration outcomes in brain. Mol. Ther. 31, 760–773.

16. Guo, T., Feng, Y.L., Xiao, J.J., Liu, Q., Sun, X.N., Xiang, J.F., Kong, N., Liu, S.C., Chen, G.Q., Wang, Y., et al. (2018). Harnessing accurate non-homologous end joining for efficient precise deletion in CRISPR/Cas9-mediated genome editing. Genome Biol. 19, 170.

17. Bosch-Guiteras, N., Uroda, T., Guillen-Ramirez, H.A., Riedo, R., Gazdhar, A., Esposito, R., Pulido-Quetglas, C., Zimmer, Y., Medová, M., and Johnson, R. (2021). Enhancing CRISPR deletion via pharmacological delay of DNA-PKcs. Genome Res. 31, 461–471.

18. Lang, J.F., Toulmin, S.A., Brida, K.L., Eisenlohr, L.C., and Davidson, B.L. (2019). Standard screening methods underreport AAV-mediated transduction and gene editing. Nat. Commun. 10, 3415.

19. Staahl, B.T., Benekareddy, M., Coulon-Bainier, C., Banfal, A.A., Floor, S.N., Sabo, J.K., Urnes, C., Munares, G.A., Ghosh, A., and Doudna, J.A. (2017). Efficient genome editing in the mouse brain by local delivery of engineered Cas9 ribonucleoprotein complexes. Nat. Biotechnol. 35, 431–434.

20. Suzuki, K., Tsunekawa, Y., Hernandez-Benitez, R., Wu, J., Zhu, J., Kim, E.J., Hatanaka, F., Yamamoto, M., Araoka, T., Li, Z., et al. (2016). In vivo genome editing via CRISPR/Cas9 mediated homology-independent targeted integration. Nature 540, 144–149.

21. Qiu, M., Glass, Z., Chen, J., Haas, M., Jin, X., Zhao, X., Rui, X., Ye, Z., Li, Y., Zhang, F., and Xu, Q. (2021). Lipid nanoparticle-mediated codelivery of Cas9 mRNA and single-guide RNA achieves liver-specific in vivo genome editing of Angptl3. Proc. Natl. Acad. Sci. USA. 118, e2020401118.

22. Li, Y., Park, A.I., Mou, H., Colpan, C., Bizhanova, A., Akama-Garren, E., Joshi, N., Hendrickson, E.A., Feldser, D., Yin, H., et al. (2015). A versatile reporter system for CRISPR-mediated chromosomal rearrangements. Genome Biol. 16, 111.

23. Watry, H.L., Feliciano, C.M., Gjoni, K., Takahashi, G., Miyaoka, Y., Conklin, B.R., and Judge, L.M. (2020). Rapid, precise quantification of large DNA excisions and inversions by ddPCR. Sci. Rep. 10, 14896.

24. Angelopoulou, A., Papaspyropoulos, A., Papantonis, A., and Gorgoulis, V.G. (2022). CRISPR-Cas9-mediated induction of large chromosomal inversions in human bronchial epithelial cells. STAR Protoc. 3, 101257.

25. Chen, F., Jimenez, R.J., Sharma, K., Luu, H.Y., Hsu, B.Y., Ravindranathan, A., Stohr, B.A., and Willenbring, H. (2020). Broad Distribution of Hepatocyte Proliferation in Liver Homeostasis and Regeneration. Cell Stem Cell 26, 27–33.e4.

26. Duncan, A.W., Taylor, M.H., Hickey, R.D., Hanlon Newell, A.E., Lenzi, M.L., Olson, S.B., Finegold, M.J., and Grompe, M. (2010). The ploidy conveyor of mature hepatocytes as a source of genetic variation. Nature 467, 707–710.

27. Monteys, A.M., Hundley, A.A., Ranum, P.T., Tecedor, L., Muehlmatt, A., Lim, E., Lukashev, D., Sivasankaran, R., and Davidson, B.L. (2021). Regulated control of gene therapies by drug-induced splicing. Nature 596, 291–295.

28. Li, A., Tanner, M.R., Lee, C.M., Hurley, A.E., De Giorgi, M., Jarrett, K.E., Davis, T.H., Doerfler, A.M., Bao, G., Beeton, C., and Lagor, W.R. (2020). AAV-CRISPR Gene Editing Is Negated by Pre-existing Immunity to Cas9. Mol. Ther. 28, 1432–1441.

29. Charlesworth, C.T., Deshpande, P.S., Dever, D.P., Camarena, J., Lemgart, V.T., Cromer, M.K., Vakulskas, C.A., Collingwood, M.A., Zhang, L., Bode, N.M., et al. (2019). Identification of preexisting adaptive immunity to Cas9 proteins in humans. Nat. Med. 25, 249–254.

30. Nelson, C.E., Wu, Y., Gemberling, M.P., Oliver, M.L., Waller, M.A., Bohning, J.D., Robinson-Hamm, J.N., Bulaklak, K., Castellanos Rivera, R.M., Collier, J.H., et al. (2019). Long-term evaluation of AAV-CRISPR genome editing for Duchenne muscular dystrophy. Nat. Med. 25, 427–432.

31. Ramaswamy, S., Tonnu, N., Tachikawa, K., Limphong, P., Vega, J.B., Karmali, P.P., Chivukula, P., and Verma, I.M. (2017). Systemic delivery of factor IX messenger RNA for protein replacement therapy. Proc. Natl. Acad. Sci. USA. 114, E1941–E1950.

32. George, L.A., Ragni, M.V., Rasko, J.E.J., Raffini, L.J., Samelson-Jones, B.J., Ozelo, M., Hazbon, M., Runowski, A.R., Wellman, J.A., Wachtel, K., et al. (2020). Long-Term Follow-Up of the First in Human Intravascular Delivery of AAV for Gene Transfer: AAV2-hFIX16 for Severe Hemophilia B. Mol. Ther. 28, 2073–2082.

33. Jiang, H., Couto, L.B., Patarroyo-White, S., Liu, T., Nagy, D., Vargas, J.A., Zhou, S., Scallan, C.D., Sommer, J., Vijay, S., et al. (2006). Effects of transient immunosuppression on adenoassociated, virus-mediated, liver-directed gene transfer in rhesus macaques and implications for human gene therapy. Blood 108, 3321–3328.

34. Li, C., Narkbunnam, N., Samulski, R.J., Asokan, A., Hu, G., Jacobson, L.J., Manco-Johnson, M.J., and Monahan, P.E.; Joint Outcome Study Investigators (2012). Neutralizing antibodies against adeno-associated virus examined prospectively in pediatric patients with hemophilia. Gene Ther. 19, 288–294.

35. Mao, Z., Bozzella, M., Seluanov, A., and Gorbunova, V. (2008). Comparison of nonhomologous end joining and homologous recombination in human cells. DNA Repair 7, 1765–1771.

36. Yamada, Y., Kamiya, H., and Harashima, H. (2005). Kinetic analysis of protein production after DNA transfection. Int. J. Pharm. 299, 34–40.

37. Leonhardt, C., Schwake, G., Stögbauer, T.R., Rappl, S., Kuhr, J.T., Ligon, T.S., and Rädler, J.O. (2014). Single-cell mRNA transfection studies: delivery, kinetics and statistics by numbers. Nanomedicine 10, 679–688.

38. Phua, K.K.L., Leong, K.W., and Nair, S.K. (2013). Transfection efficiency and transgene expression kinetics of mRNA delivered in naked and nanoparticle format. J. Contr. Release 166, 227–233.

39. He, Y., Weinberg, M.S., Hirsch, M., Johnson, M.C., Tisch, R., Samulski, R.J., and Li, C. (2013). Kinetics of adeno-associated virus serotype 2 (AAV2) and AAV8 capsid antigen presentation in vivo are identical. Hum. Gene Ther. 24, 545–553.

40. Malik, A.K., Monahan, P.E., Allen, D.L., Chen, B.G., Samulski, R.J., and Kurachi, K. (2000). Kinetics of recombinant adeno-associated virus-mediated gene transfer. J. Virol. 74, 3555–3565.

41. Pardi, N., Tuyishime, S., Muramatsu, H., Kariko, K., Mui, B.L., Tam, Y.K., Madden, T.D., Hope, M.J., and Weissman, D. (2015). Expression kinetics of nucleoside-modified mRNA delivered in lipid nanoparticles to mice by various routes. J. Contr. Release 217, 345–351.

42. Musunuru, K., Chadwick, A.C., Mizoguchi, T., Garcia, S.P., DeNizio, J.E., Reiss, C.W., Wang, K., Iyer, S., Dutta, C., Clendaniel, V., et al. (2021). In vivo CRISPR base editing of PCSK9 durably lowers cholesterol in primates. Nature 593, 429–434.

43. Powars, D.R., Weiss, J.N., Chan, L.S., and Schroeder, W.A. (1984). Is there a threshold level of fetal hemoglobin that ameliorates morbidity in sickle cell anemia? Blood 63, 921–926.

44. Esrick, E.B., Lehmann, L.E., Biffi, A., Achebe, M., Brendel, C., Ciuculescu, M.F., Daley, H., MacKinnon, B., Morris, E., Federico, A., et al. (2021). Post-Transcriptional Genetic Silencing of BCL11A to Treat Sickle Cell Disease. N. Engl. J. Med. 384, 205–215.

45. Tombácz, I., Laczkó, D., Shahnawaz, H., Muramatsu, H., Natesan, A., Yadegari, A., Papp, T.E., Alameh, M.G., Shuvaev, V., Mui, B.L., et al. (2021). Highly efficient CD4+ T cell targeting and genetic recombination using engineered CD4+ cell-homing mRNA-LNPs. Mol. Ther. 29, 3293–3304.

46. Shi, D., Toyonaga, S., and Anderson, D.G. (2023). In Vivo RNA Delivery to Hematopoietic Stem and Progenitor Cells via Targeted Lipid Nanoparticles. Nano Lett. 23, 2938–2944.

47. Bonafont, J., Mencía, Á., García, M., Torres, R., Rodríguez, S., Carretero, M., Chacón-Solano, E., Modamio-Høybjør, S., Marinas, L., León, C., et al. (2019). Clinically Relevant Correction of Recessive Dystrophic Epidermolysis Bullosa by Dual sgRNA CRISPR/Cas9-Mediated Gene Editing. Mol. Ther. 27, 986–998.

48. Sanz, D.J., Hollywood, J.A., Scallan, M.F., and Harrison, P.T. (2017). Cas9/gRNA targeted excision of cystic fibrosis-causing deep-intronic splicing mutations restores normal splicing of CFTR mRNA. PLoS One 12, e0184009.

49. Meijboom, K.E., Abdallah, A., Fordham, N.P., Nagase, H., Rodriguez, T., Kraus, C., Gendron, T.F., Krishnan, G., Esanov, R., Andrade, N.S., et al. (2022). CRISPR/Cas9-mediated excision of ALS/FTD-causing hexanucleotide repeat expansion in C9ORF72 rescues major disease mechanisms in vivo and in vitro. Nat. Commun. 13, 6286.

50. Ito, Y., Remion, A., Tauzin, A., Ejima, K., Nakaoka, S., Iwasa, Y., Iwami, S., and Mammano, F. (2017). Number of infection events per cell during HIV-1 cell-free infection. Sci. Rep. *7*, 6559.

51. Wang, J., Xu, Z.W., Liu, S., Zhang, R.Y., Ding, S.L., Xie, X.M., Long, L., Chen, X.M., Zhuang, H., and Lu, F.M. (2015). Dual gRNAs guided CRISPR/Cas9 system inhibits hepatitis B virus replication. World J. Gastroenterol. *21*, 9554–9565.

52. Kaminski, R., Bella, R., Yin, C., Otte, J., Ferrante, P., Gendelman, H.E., Li, H., Booze, R., Gordon, J., Hu, W., and Khalili, K. (2016). Excision of HIV-1 DNA by gene editing: a proof-of-concept in vivo study. Gene Ther. *23*, 696.

53. Cataldi, M.P., and McCarty, D.M. (2010). Differential effects of DNA double-strand break repair pathways on single-strand and self-complementary adeno-associated virus vector genomes. J. Virol. *84*, 8673–8682.

54. Bond, S.T., Zhuang, A., Yang, C., Gould, E.A.M., Sikora, T., Liu, Y., Fu, Y., Watt, K.I., Tan, Y., Kiriazis, H., et al. (2021). Tissue-specific expression of Cas9 has no impact on whole-body metabolism in four transgenic mouse lines. Mol. Metabol. *53*, 101292.

55. Link, R.W., Nonnemacher, M.R., Wigdahl, B., and Dampier, W. (2018). Prediction of Human Immunodeficiency Virus Type 1 Subtype-Specific Off-Target Effects Arising from CRISPR-Cas9 Gene Editing Therapy. CRISPR J. *1*, 294–302.

56. Hendel, A., Fine, E.J., Bao, G., and Porteus, M.H. (2015). Quantifying on- and off-target genome editing. Trends Biotechnol. *33*, 132–140.

57. Wang, Y., Wei, D., Zhu, X., Pan, J., Zhang, P., Huo, L., and Zhu, X. (2016). A 'suicide' CRISPR-Cas9 system to promote gene deletion and restoration by electroporation in Cryptococcus neoformans. Sci. Rep. *6*, 31145.

58. Li, A., Lee, C.M., Hurley, A.E., Jarrett, K.E., De Giorgi, M., Lu, W., Balderrama, K.S., Doerfler, A.M., Deshmukh, H., Ray, A., et al. (2019). A Self-Deleting AAV-CRISPR System for In Vivo Genome Editing. Mol. Ther. Methods Clin. Dev. *12*, 111–122.

59. Hakim, C.H., Kumar, S.R.P., Pérez-López, D.O., Wasala, N.B., Zhang, D., Yue, Y., Teixeira, J., Pan, X., Zhang, K., Million, E.D., et al. (2021). Cas9-specific immune responses compromise local and systemic AAV CRISPR therapy in multiple dystrophic canine models. Nat. Commun. *12*, 6769.

60. Moreno, A.M., Palmer, N., Alemán, F., Chen, G., Pla, A., Jiang, N., Leong Chew, W., Law, M., and Mali, P. (2019). Immune-orthogonal orthologues of AAV capsids and of Cas9 circumvent the immune response to the administration of gene therapy. Nat. Biomed. Eng. *3*, 806–816.

61. Nguyen, G.N., Everett, J.K., Kafle, S., Roche, A.M., Raymond, H.E., Leiby, J., Wood, C., Assenmacher, C.A., Merricks, E.P., Long, C.T., et al. (2021). A long-term study of AAV gene therapy in dogs with hemophilia A identifies clonal expansions of transduced liver cells. Nat. Biotechnol. *39*, 47–55.

62. Carrasco, M.J., Alishetty, S., Alameh, M.G., Said, H., Wright, L., Paige, M., Soliman, O., Weissman, D., Cleveland, T.E., 4th, Grishaev, A., and Buschmann, M.D. (2021). Ionization and structural properties of mRNA lipid nanoparticles influence expression in intramuscular and intravascular administration. Commun. Biol. *4*, 956.

63. Jozefczuk, J., Drews, K., and Adjaye, J. (2012). Preparation of mouse embryonic fibroblast cells suitable for culturing human embryonic and induced pluripotent stem cells. J. Vis. Exp. *64*, 3854.